HAL
open science

Rock walls distribution and Holocene evolution in a mid-latitude mountain range (the Romanian Carpathians)

Mirela Vasile, Alfred Vespremeanu-Stroe, Daniela Pascal, Regis Braucher, Alin Pleșoianue, Răzva Popescu, Bernd Etzelmüller

To cite this version:

Mirela Vasile, Alfred Vespremeanu-Stroe, Daniela Pascal, Regis Braucher, Alin Pleșoianue, et al.. Rock walls distribution and Holocene evolution in a mid-latitude mountain range (the Romanian Carpathians). Geomorphology, 2022, pp.108351. 10.1016/j.geomorph.2022.108351 . hal-03702052

HAL Id: hal-03702052

https://amu.hal.science/hal-03702052v1

Submitted on 22 Jun 2022

HAL is a multi-disciplinary open access archive for the deposit and dissemination of scientific research documents, whether they are published or not. The documents may come from teaching and research institutions in France or abroad, or from public or private research centers.

L'archive ouverte pluridisciplinaire **HAL**, est destinée au dépôt et à la diffusion de documents scientifiques de niveau recherche, publiés ou non, émanant des établissements d'enseignement et de recherche français ou étrangers, des laboratoires publics ou privés.

Geomorphology

Rock walls distribution and Holocene evolution in a mid-latitude mountain range (the Romanian Carpathians)

--Manuscript Draft--

Manuscript Number:	GEOMOR-11671
Article Type:	Research Paper
Keywords:	rock wall morphometry; lithology; rock slope failures; Romanian Carpathians
Abstract:	Rock walls in high mountain areas are the expression of long–term slopes response (10 3 –10 5 years) to tectonics, weathering and denudation and a major source of sediment and hazard. Mountain rock walls (RW) characteristics and evolution at mountain–range scale is rarely discussed in the literature. Using a database of 791 RW mapped in the Romanian Carpathians, we present their distribution and morphometry in respect to lithological class, structural features and topography and relate them to post–Younger Dryas (Holocene) rock slope failure chronology. Morphometric data indicate that metamorphic and igneous RW (linked to a great extent to glacial valleys and cirques headwalls) are usually restricted to the highest sectors of the mountain slopes, are characterized by reduced relative heights and have an asymmetrical distribution, being common on the North-exposed slopes but extremely rare on the South. Statistical analysis results show the high significance of structural and tectonic control on RW distribution in sedimentary units which imposes the predominance of West and North orientations and RW dimensions up to a degree higher than in other lithologies. Based on 38 10 Be surface exposure ages obtained on metric boulders from the Southern and Eastern Carpathians, we hypothesise that metamorphic and igneous RW in the formerly glaciated Carpathian valleys were significantly shaped during Early Holocene (before 9 ka) by rock slope failures events that followed the deglaciation of the highest cirques and the intense RW permafrost degradation. We associate the long–term imprints of frost weathering to the significant North/South RW and rock glaciers distribution asymmetry, also identified in other mid-latitude mountain sites with similar topographic constraints.

Powered by Editorial Manager® and ProduXion Manager® from Aries Systems Corporation

Abstract

Rock walls in high mountain areas are the expression of long–term slopes response (10^3–10^5 years) to tectonics, weathering and denudation and a major source of sediment and hazard. Mountain rock walls (RW) characteristics and evolution at mountain–range scale is rarely discussed in the literature. Using a database of 791 RW mapped in the Romanian Carpathians, we present their distribution and morphometry in respect to lithological class, structural features and topography and relate them to post–Younger Dryas (Holocene) rock slope failure chronology. Morphometric data indicate that metamorphic and igneous RW (linked to a great extent to glacial valleys and cirques headwalls) are usually restricted to the highest sectors of the mountain slopes, are characterized by reduced relative heights and have an asymmetrical distribution, being common on the North-exposed slopes but extremely rare on the South. Statistical analysis results show the high significance of structural and tectonic control on RW distribution in sedimentary units which imposes the predominance of West and North orientations and RW dimensions up to a degree higher than in other lithologies. Based on 38 ^{10}Be surface exposure ages obtained on metric boulders from the Southern and Eastern Carpathians, we hypothesise that metamorphic and igneous RW in the formerly glaciated Carpathian valleys were significantly shaped during Early Holocene (before 9 ka) by rock slope failures events that followed the deglaciation of the highest cirques and the intense RW permafrost degradation. We associate the long–term imprints of frost weathering to the significant North/South RW and rock glaciers distribution asymmetry, also identified in other mid-latitude mountain sites with similar topographic constraints.

TITLE: Rock walls distribution and Holocene evolution in a mid-latitude mountain range (the Romanian Carpathians)

Authors:

Mirela Vasile[*a], Alfred Vespremeanu-Stroe[a,b], Daniela Pascal[b,c], Regis Braucher[d] , Alin Plișoianu[e], Răzvan Popescu[a,b], Bernd Etzelmüller[f]

Affiliations:

[a] Research Institute of the University of Bucharest, 90-92 Sos. Panduri, 050663, sector 5, Bucharest, Romania

[b] Faculty of Geography, University of Bucharest, 1 N. Bălcescu Blv., 010041, sector 1, Bucharest, Romania

[c] Horia Hulubei National Institute for R&D in Physics and Nuclear Engineering, 30 Aleea Reactorului Str., 077125, Măgurele, Romania

[d] Aix-Marseille Univ., CEREGE, CNRS-IRD-Collége de France-INRAE BP 80, 13545 Aix-en-Provence Cedex 4, France

[e] ESRI Romania, 25 Washington Str., sector 1, Bucharest, Romania

[f] Department of Geosciences, University of Oslo, 1047, Blindern, Oslo, Norway

Corresponding Author:

Mirela Vasile, Research Institute of the University of Bucharest, 90-92 Sos. Panduri, 050663, sector 5, Bucharest, Romania, mirela.vasile@geo.unibuc.ro

ABSTRACT

Rock walls in high mountain areas are the expression of long–term slopes response (10^3–10^5 years) to tectonics, weathering and denudation and a major source of sediment and hazard.

Mountain rock walls (RW) characteristics and evolution at mountain–range scale is rarely discussed in the literature. Using a database of 791 RW mapped in the Romanian Carpathians, we present their distribution and morphometry in respect to lithological class, structural features and topography and relate them to post–Younger Dryas (Holocene) rock slope failure chronology. Morphometric data indicate that metamorphic and igneous RW (linked to a great extent to glacial valleys and cirques headwalls) are usually restricted to the highest sectors of the mountain slopes, are characterized by reduced relative heights and have an asymmetrical distribution, being common on the North-exposed slopes but extremely rare on the South. Statistical analysis results show the high significance of structural and tectonic control on RW distribution in sedimentary units which imposes the predominance of West and North orientations and RW dimensions up to a degree higher than in other lithologies. Based on 38 ^{10}Be surface exposure ages obtained on metric boulders from the Southern and Eastern Carpathians, we hypothesise that metamorphic and igneous RW in the formerly glaciated Carpathian valleys were significantly shaped during Early Holocene (before 9 ka) by rock slope failures events that followed the deglaciation of the highest cirques and the intense RW permafrost degradation. We associate the long–term imprints of frost weathering to the significant North/South RW and rock glaciers distribution asymmetry, also identified in other mid-latitude mountain sites with similar topographic constraints.

KEYWORDS: rock wall morphometry; lithology; rock slope failures; Romanian Carpathians

1. INTRODUCTION

Mountain RW are landforms highly sensitive for mechanical weathering and erosional processes (Hales and Roering, 2007; Matsuoka, 2008; Allen and Huggel, 2013; Phillips *et al.*, 2017), the rates of which are dictated by the interplay of lithology, climate and the local uplift regime (Willett 1999; Seong et al. 2009; Bartosch et al. 2017). Tectonics and structure significantly influence the extent and morphometry of the exposed rock surfaces in high

mountain areas (Lifton et al. 2009; Ellis and Barnes 2015; Sauchyn et al. 1998) which determine differential resistance to weathering and erosion. In formerly glaciated European mountain ranges, weathering and denudation rates are reported quantitatively after the Last Glacial period (Curry and Morris 2004; Hughes et al. 2007; Messenzehl et al. 2017; Matthews et al. 2018). The occurrence of numerous rock slope failures (RSF) in response to local deglaciation debuttressing has been documented by absolute age dating (Soldati et al., 2004; Prager *et al.*, 2008; Ballantyne *et al.*, 2014) with responses varying from immediate to millennial time lags (Ballantyne *et al.*, 2014). The reconstruction of RSF chronology in Tatra Mountains (Pánek *et al.*, 2016) shows that lower magnitude events within steep topography occurred in the highest sectors of slopes hundreds of years after glacier retreat and are likely triggered by ice mass disappearance, whereas complex RSF producing at millennial time–scale in lower topography are associated with climate changing to warmer and more humid conditions during the onset of the Holocene and the Sub-Boreal period (Soldati et al., 2004; Ivy-Ochs *et al.*, 2009; Hermanns and Longva, 2013).

High–mountain rock slopes are a continuous source area for geomorphic processes that trigger natural hazards like debris flows, rockfalls or rock avalanches (Loye et al. 2009; Corona et al. 2013; Kromer 2017), especially when affected by permafrost degradation. RW stability is responsive to climate variables such as changes of permafrost conditions (Krautblatter et al. 2013; Girard et al. 2013) and global climate change influencing periglacial processes (Gruber et al., 2004; Messenzehl *et al.*, 2017; Phillips *et al.*, 2017), which has also been documented in warming conditions during the Holocene in the European and Scandinavian Alps (Hormes *et al.*, 2008; Nagelisen *et al.*, 2015; Hilger *et al.*, 2021). This raises the question of RW evolution and subsequent debris production induced by the post–Younger Dryas permafrost retreat, especially in mid-latitude where permafrost in northerly slopes exists at lower altitudes than in southerly slopes (Magnin *et al.*, 2015).

Range–scale morphometric studies in the Romanian Carpathians have been documenting the distribution of glacial cirques by high–accuracy mapping (Mîndrescu and Evans 2014; Mîndrescu et al. 2010) and object oriented image analysis (Ardelean 2013). Geochronology studies based on absolute ages resume to deglaciation history, pointing to a Younger Dryas glacial advance at 12.9–12.1 ka only in the highest massifs (Popescu et al., 2017a). During the last decade, the intensive monitoring of the thermal regime of permafrost susceptible sites has shown the restrictive conditions for permafrost preservation in RW and rock glaciers (Vespremeanu–Stroe et al., 2012; Ardelean *et al.*, 2017; Onaca *et al.*, 2017; Popescu *et al.*, 2017b). Recent studies on RW present state, in terms of stability or thermal regime, emphasized the rockfall hazard imposed by seasonal thawing in steep North–exposed RW (Vasile et al., 2014; Onaca *et al.*, 2015; Vasile and Vespremeanu–Stroe, 2017).

In this paper we i) present the distribution of RW in relation to lithology, structure and topography for assessing differential RW retreat control factors and ii) provide a first insight on Holocene RSF occurrence as the last major shaping agent of RW in the Romanian Carpathians. The objectives are achieved by RW mapping and statistical analysis of distribution controlling parameters, and by in-situ ^{10}Be surface exposure data analysis in glacial cirques and valleys from five different massifs.

2. STUDY AREA

The Romanian Carpathians stand as a geographical subdivision of the Carpathian Mountain Arc that stretches in Central and Eastern Europe (44° 30’ – 47° 45’ N and 21° 30’ – 27° 10’ E). They expand to a length of 900 km and reach the maximum altitude of 2544 m above sea level (a.s.l.). The three main subdivisions (i.e., the Eastern and Southern Carpathians – abbreviated EC and SC further on – and the Apuseni Mountains, Fig. 1a, b) show lithological and topographic differences that reflect the complexity of the geological evolution, structural characteristics, and influence of the Pleistocene glaciations.

The Carpathians are part of the Alpine Orogeny and include tectonic units dating prior to the alpine event, in the Palaeozoic and early Mesozoic. The youngest exhumation phases determined by thermochronology age patterns in the central part of the SC are Latest Cretaceous – Middle Eocene. The south–western sector of the SC underwent Oligocene – Miocene exhumation, whereas most of the EC correspond to Early – Middle Miocene phases, except for the SE Carpathians (Curvature Carpathians) which started uplifting in both Miocene and Latest Pliocene – Quaternary exhumation episodes (Merten, 2011). The EC are built on a central Crystalline Unit (correspondent to present Rodna, Maramureș, Rarău and Hășmaș Mts.), Cretaceous Flysch (Ceahlău and Ciucaș Mts, extending towards the SC in Bucegi Mts) and Palaeogene Flysch (Table 1, Fig. 1b). Internal volcanism during the Miocene led to the formation of EC volcanic massifs while the Pliocene – Quaternary comprised both a rapid uplift of 500–1000 m (which led to the formation of the most recent depression areas), and the strongest volcanic activity in the area (Săndulescu, 1984; Linzer *et al.*, 1998; Mutihac, 2004). The SC are comprised of three major Crystalline Units: the Getic Overthrust Nappe (Șureanu, Căpățânii, Lotru, Cindrel, Godeanu Mts), the Supragetic Overthrust Nappe (Făgăraș and Iezer Mts) and the Danubian Nappes (Retezat and Parâng Mts), the latter being formed by granitic and granodioritic batholiths in their central areas and marginal limestone massifs (Fig. 1a, b for location, Table 1).

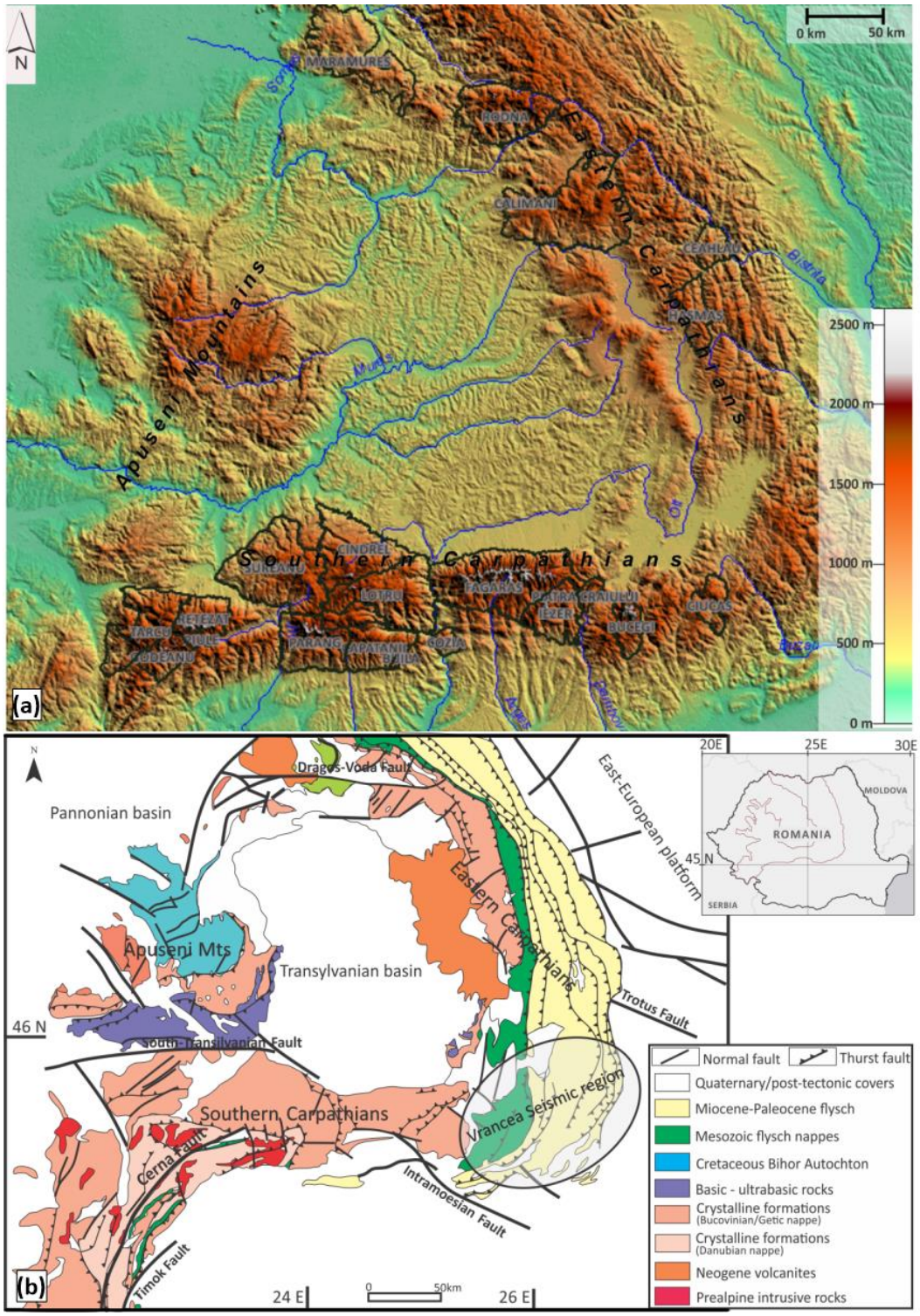

Figure 1: (a) Location of Eastern and Southern Carpathians and Apuseni Mts., and outline of the units included in the RW inventory (digital elevation by 1 arc-second resolution ASTER GDEM). (b) Simplified geological map of the Carpathians (modified and adapted from Vaida and Verniers, 2005, and Merten, 2011. Small insert shows the Carpathian Arc position in Romania (please refer to the colour version)

	Unit name (max. altitude)	Lithology/ Structure*	Extent / Direction	Nr. of mapped RW	Glaciation**
Eastern Carpathians	Maramureş (1956 m)	Crystalline schist with peripheral limestone and sandstones Volcanic intrusions (basalts)	15 km long / NW–SE ridge	11	Yes
	Rodna (2303 m)	Crystalline schist, micaschists and paragneiss Horst, Dragoş Vodă Fault	40 km long / E–W ridge	19	Yes
	Călimani (2100 m)	Andesites (volcanic) Eroded craters	Volcanic cone	5	Yes
	Ceahlău (1969 m)	Conglomerates and flysch Suspended syncline	15 km / N–S	10	No
	Hăşmaş (1973 m)	Massive limestone West oriented syncline	3.5 km long / NW–SE ridge	6	No
	Ciucaş (1954 m)	Conglomerates and sandstones, flysch East oriented syncline	Two separated ridges 7 km / SW–NE and 3 km / NW–SE	37	No
Southern Carpathians	Bucegi (2505 m)	Conglomerates, sandstones Limestone with radiolarites N–S syncline, East oriented cuesta front slope	Reversed U–shape 30 km long ridge	49	Yes
	Piatra Craiului (2238 m)	Limestone with radiolarites Hogback	25 km long / NNE–SSW ridge	13	No
	Iezer (2459 m)	Micaschists and paragneiss Supragetic overthrust nappe	20 km long / SW–NE ridge	27	Yes
	Făgăraş (2544 m)	Micashists and paragneiss, amphibolite Supragetic overthrust nappe Northern–Făgăraş Fault Line	70km long W–E ridge, and multiple secondary N–S ridges	248	Yes
	Cozia (1668 m)	Gneiss Horst	~70 km^2 surface	3	No
	Buila–Vânturariţa (1885 m)	Massive Limestone Hogback	14 km long / SW–NE ridge	23	No
	Parâng (2519 m)	Granitoids Amphibolite (Danubian Unit)	25 km long / E–W ridge	40	Yes
	Şureanu/ Cindrel/ Căpăţânii/ Lotrului (2130 – 2244 m)	Micaschists and paragneiss, amphibolite (Getic Unit)	15–25 km long / E–W ridges	8 / 10/ 4 / 5	Yes
	Retezat (2509 m)	Granodiorite intrusions Crystalline schist, amphibolite (Danubian Unit)	15 km long main / W–E ridge 2–5 km secondary N–S ridges	187	Yes
	Ţarcu (2196 m)	Conglomerates, sandstones, crystalline limestone Crystalline schist	20 km long / N–S then NE–SW ridge	26	Yes
	Godeanu/ Piule Iorgovanul (2291 m)	Micaschists and paragneiss, amphibolite / Recifal limestone	20 km long / NE–SW ridge	26 / 13	Yes
	Cerna Valley (1200 m)	Recifal limestone Graben	80 km long valley / NS	21	No

Table 1: Main lithological, structural and morphographic characteristics of the mountain units in which rock walls were mapped

* according to the Geological Map of Romania, scale 1:200 000 (Geological Institute of Romania)

** according to the Map of Glacial Cirques in the Romanian Carpathians (Mîndrescu, 2016)

Present neo–tectonic movements show a differential uplift trend of the Carpathian orogeny with mean values of 1–3 mm/yr, higher values up to 3–5 mm/yr reported in the Eastern Făgăraş, Bucegi Mts. and the Curvature Carpathians which are associated with the activity from Vrancea seismic region (Hoeven *et al.*, 2005).

The past glacial activity in the Carpathian area is expressed by well–preserved glacial cirques, valleys and associated rock walls (Mîndrescu et al., 2010), most of which were modelled during LGM and Late Glacial cold phases (Popescu et al. 2017a).

The Romanian Carpathians are characterized by a temperate–continental climate, the mean annual air temperature (MAAT) ranging from -2°C at 2500 m a.s.l. (Vf. Omu meteorological station) and -0.4°C at 2190 m a.s.l. (Țarcu station) to 3 °C at 1577 m a.s.l. (Cozia station). Using a lapse rate of 0.63°C/100 m, the 0°C MAAT isotherm is around 2000 m a.s.l. on North–facing slopes and 2100 m a.s.l. on South–facing ones. Moisture is supplied by the West and SW dominating winds originating in the North–Atlantic and the Mediterranean, mean annual rainfall above 2000 m is 1100–1300 mm, snow cover reaches 1.5–2.0 m during January–March, and lasts in average 150–160 days per season (Micu *et al.*, 2015). In-situ RW thermal monitoring above 2200 m a.s.l. (Vasile and Vespremeanu-Stroe, 2017) exhibits prolonged seasonal frost (140–150 days/season with potential frost penetration depths reaching 2 m), and mean annual rock temperatures (MART) of 0.5°C on the North–exposed slopes and 3–4°C higher MART on the southern slopes, where daily temperature oscillations prevail, and continuous freezing rarely sets within the -3…-8°C freezing window.

3. METHODS AND DATA

3.1 Rock wall mapping

RW were mapped based on the available time records of Google Earth satellite imagery. Because some images were not clear enough for a good differentiation between the RW and the adjacent geomorphological units, a comparison with higher resolution air photography was undertaken (orthophoto images available for view only from the National Agency for Cadastre and Land Legislation – ANCPI at 1–5 m resolution). Further, the 25 m resolution EU–DEM digital surface model (EEA) was used to check slopes inclination and the inflection points within longitudinal profiles at the contact with the talus or at the top of the glacial cirques. The term

rock wall refers herein to steep, bare and compact rock surfaces, with angles usually higher than 37–40 degrees (Gruber, 2007). We took into account RW with areas larger than 200 m^2 in order to avoid patchy rock surfaces partially covered with vegetation or sporadic discontinuous outcrops. Considering these constraints, the analysis resumes to 21 mountain units in the EC and the SC (Fig. 1a for location), where rock surfaces matching these criteria were identified on satellite imagery. The geological map of Romania (scale 1: 200 000, Geological Institute of Romania) was used to determine the rock type of each mapped RW, assuring a complete spatial coverage over the entire range.

3.2 Rock wall morphometry

Mean RW area, total coverage, altitude, relative height, orientation and slope values were computed for each mountain unit (Table 2) and per lithology types, using the values from all units developed on the same rock class (sedimentary, igneous, metamorphic or volcanic). Each RW was vectorized and the resulting polygons were overlaid on the DEMs and then used for calculating the morphometric parameters in ArcGIS software. Mean RW orientation was determined by averaging raster direction. The RW area was calculated for a 2D projection of the RW polygons on the EU–DEM.

3.3 Statistical analysis

The statistical analysis was performed in RStudio (R version 3.4.0), and consisted in three stages. First, a data normality check was performed using the Shapiro–Wilk normality test (Shapiro and Wilk, 1965), which indicated the non-normality of the data. Then, for each mountain unit, a Kruskal–Wallis one–way analysis of variance test (Kruskal and Wallis, 1952) was performed in order to check if there are any statistically significant differences between groups of quantitative parameters, namely the relations between exposures and morphometry, and between lithology and morphometry. The Kruskal-Wallis Test is the non-parametric alternative to ANOVA (one-way analysis of variance), which checks if the analysed groups are

subsets from the same population. The test computes the rank variance of the interest variable for the combined groups, and then calculates the H statistic (Equation 1)

$$H = \frac{N-1(gn_n(t_i-T_j)^2}{gsn_n(t_j-T_i)^2)}, \qquad \text{Equation (1)}$$

where n_n is the sample size of the group, g is the sum of the group n, sn_n is the sum of the corresponding group n, t_i is the average observed rank sums for the group, t_j is the observed rank for a value in the corresponding group, and T_i is the observed total average rank sums. (McKight and Najab, 2010). The computed H statistic then indicates whether the groups come from the same population by comparing it to a critical value, which for our analysis corresponds to a 95% confidence or a p-value < 0.05. For H values beyond the critical threshold the Kruskal-Wallis Test indicates strong differences between analysed groups. Finally a post–hoc Dunn's Test (Dunn, 1961) for multiple comparisons was performed in order to identify which mountain units have significantly different values of each pair of the analysed parameters.

3.4 Surface exposure ages

24 boulders (20 from Făgăraș and four from Bucegi Mts) were sampled for cosmogenic ^{10}Be exposure dating. The samples are part of an extensive study regarding deglaciation and RSF, which counts more than 120 rock surfaces (unpublished data). During sample processing, the abundance of post–Younger Dryas resulting ages raised questions about RSF triggering the detachment of such boulders, as documented in other European mountain ranges (synthesis of studies in Pánek *et al.*, 2016). The samples included in the present study were collected along 7 glacial valleys in Făgăraș Mts and one valley in Bucegi Mts, ranging from 1205 to 2287 m a.s.l., on metric–size boulders from both valley/cirque centre and peripheral. Sample size varied from 2 to 3 cm thick and sampled rock surfaces were vegetation free. Additionally, we accounted other 14 post–Younger Dryas boulder ages documented in the literature in Rodna (Gheorghiu, 2012), Parâng (Gheorghiu *et al.*, 2015) and Retezat massifs (Reuther *et al.*, 2007;

Ruszkiczay-Rüdiger *et al.*, 2021) which were considered as outliers in studies regarding deglaciation chronology, raising the database to 38 values from 16 valleys/cirques.

Secondary, we aimed for absolute dating of a rock glacier (Doamnei RG) surface in Făgăraș Mts., where we sampled four boulders from the RG body on a longitudinal profile but also the source RW area above; for comparing a North/South RW exposure, the corresponding South–face of Doamnei RW was also sampled.

Dating procedure for Făgăraș and Bucegi samples is described below.

The sample purification followed the procedure of Merchel and Herpers, 1999. Samples were crushed and sieved to the 0.25 – 1 mm fraction. Magnetic separation was performed on all samples with a magnetic separator “Frantz LB-1”. The other minerals that are embedded in samples were eliminated with mixtures of HCl and H_2SiF_6. Then atmospheric ^{10}Be was eliminated by HF (48%) dissolutions. Before the total dissolution, 150 mg of a ^{9}Be carrier solution (concentration 3025 ± 9 µg/g; Merchel *et al.*, 2008) manufactured in-house from a phenakite crystal were added to the samples. The total dissolution of quartz was performed with HF 48% (3.6 mL per g of quartz and 30 mL in excess). The resulting solutions were evaporated until dryness and samples were recovered with hydrochloric acid. Subsequently samples were precipitated with ammonia before successive separations through an anion exchange column (Dowex 1X8) to remove iron and a cation exchange column (Dowex 50WX8), and to discard boron and recover Be (Merchel and Herpers, 1999). BeO targets were prepared by mixing Niobium powder with the BeO oxide for AMS measurements.

All samples were chemically performed at *Laboratoire National des Nucléides Cosmogéniques* (LN2C) at CEREGE (Aix en Provence, France) and targets of purified BeO were prepared for AMS measurement at *ASTER, the French National AMS Facility* (CEREGE, Aix en Provence). The measurements were calibrated against an In-House standard (STD11) Braucher *et al.*, 2015 standard, using an assigned $^{10}Be/^{9}Be$ ratio of (1.191) × 10^{-11} (1.09%). Analytical

uncertainties (reported as 1ϭ) included for all samples. The ^{10}Be half-life of (1.387±0.01) × 10^6 years (Chmeleff *et al.*, 2010) was used.

Production rates were scaled following Stone, 2000 with a sea level high latitude production rate of 4.02±0.36 atoms/g SiO2/yr (Borchers *et al.*, 2016). Rock density of 2.5 g/cm^3 was used for all samples. Topographic shielding was calculated using the CosmoCalc 2.2 Excel add-in of Vermeesch, 2007. Air pressure used is 1013 mBar. There was no quantitative information on the snow cover during the surface exposure duration, hence, no corrections for potential effects of snow cover or denudation were applied to the ages. ^{10}Be exposure ages were calculated following Equation (2) using muogenic contributions of Braucher *et al.*, 2011.

$$N(x,\varepsilon,t) = \frac{Psp * \exp(-\frac{x}{Ln})(1-\exp(-t\left(\frac{\varepsilon}{Ln}+\lambda\right)}{\frac{\varepsilon}{Ln}+\lambda}$$

$$+\frac{P\mu slow * \exp(-\frac{x}{L\mu slow})(1-\exp(-t(\frac{\varepsilon}{L\mu slow}+\lambda)}{\frac{\varepsilon}{L\mu slow}+\lambda}$$

$$+\frac{P\mu fast * \exp(-\frac{x}{L\mu fast)})(1-\exp(-t(\frac{\varepsilon}{L\mu fast}+\lambda)}{\frac{\varepsilon}{L\mu fast}+\lambda}$$

Equation (2)

where:

N (x, ε, t) is the nuclide concentration function of depth *x* (g/cm^2), denudation rate *ε* (g/cm^2/y) and exposure time *t*(y). *Psp, Pμslow, Pμfast* and *Ln, Lμslow, Lμfast* are the production rates and attenuation lengths of neutrons, slow muons and fast muons, respectively. *Ln, Lμslow, Lμfast* values used are 160, 1500 and 4320 g/cm^2, respectively Braucher *et al.*, 2003. *λ* is the radioactive decay constant. Pμslow, Pμfast are based on Braucher *et al.*, 2011.

4. RESULTS

4.1 RW distribution

From the 21 units considered in this study, 11 preserve glacial landforms (Table 1). In the EC, only Rodnei, Maramureş, and Călimani massifs present visible glacial landforms (cirques, valleys and moraine deposits), most of which are in Rodnei Mts. (Mîndrescu 2016). The best preserved landforms are in Făgăraş Mts., where 207 glacial cirques were mapped (Mîndrescu et al. 2010), in Retezat Mts., which show extensive moraine deposits, glacial lakes and complex glacial valleys (Urdea, 2000), and in Parâng Mts., which keep the largest glacial cirques in the Romanian Carpathians (Iancu, 1970). The distribution of glacial cirques in the SC particularly reflects the main ridge orientation, with moderate differences of frequencies between North and South–exposed cirques (17% on North and 11% on South respectively, reported to 45 degrees bins) and the most favourable conditions of cirque glaciers formation on the East–exposed slopes of the valleys (19.5%) due to the strong eastward aeolian snow-transport acting on the crests and plateaus (Vespremeanu-Stroe et al., 2012). In terms of area and height, the North exposures preserve generally larger and wider cirques (Mîndrescu 2016).

A total of 791 RW were identified and considered as individual features, most of which were mapped in the SC. In most of the mountain units considered here, the main ridges follow East–West or NE–SW direction (Table 1), tracking the principal fault lines (Fig. 1a, b). The distribution of the RW is further presented, based on mean orientation and RW altitude.

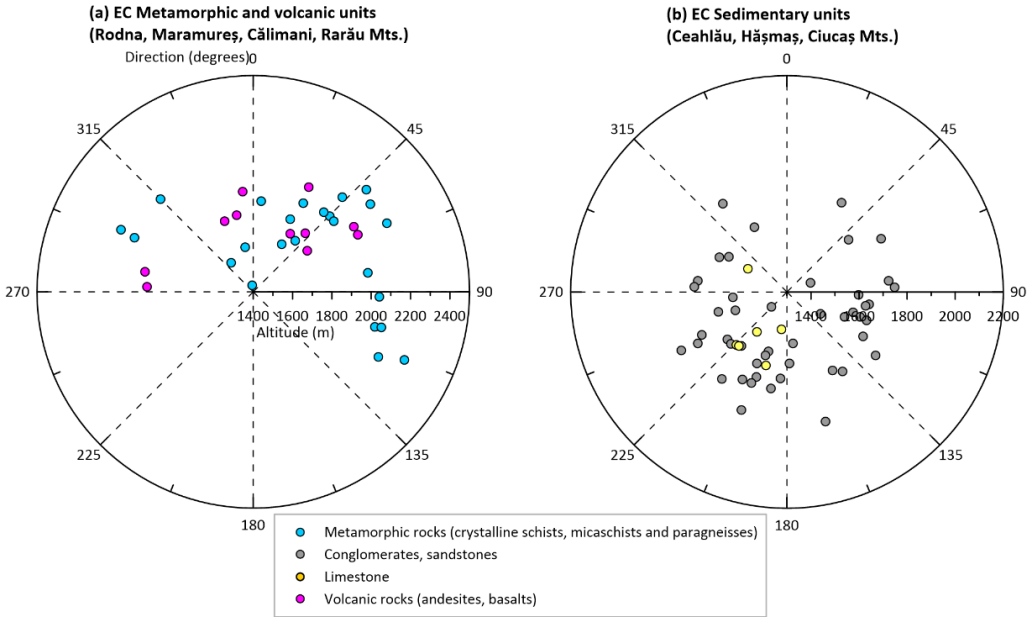

Figure 2: Direction and mean altitude of the RW mapped in the EC: (a) the metamorphic schists – prevailing units; the andesitic and basaltic outcrops are represented as volcanic RW; (b) the sedimentary units (limestone and conglomerates prevailing). The radius of the graphs represents the altitude values, the general direction is expressed in sexagesimal degrees and each dot represents a RW (please refer to the colour version)

The units from the EC count 88 mapped RW in total. The RW found in the schist–prevailing massifs are distributed mainly on NE (23%) and secondary on North and East (Fig. 2a) with an average altitude of 1950 m a.s.l., the North–exposed ones being situated at slightly lower altitudes. The andesitic and basaltic rock outcrops mapped in the EC, are largely grouped on the North and NE (82%) similarly with the metamorphic ones.

In the sedimentary units, RW extend on all orientations, with a maximum frequency on the South (almost 40%) whilst just a few (7%) were mapped on the northern slopes (Fig. 2b), but are limited to altitudes lower than 1800 m, reaching an average of 1634 m a.s.l. which is considerably lower (> 300 m) than the metamorphic and volcanic RW.

Compared to the EC, the number of RW mapped in the mountain units from the SC built on metamorphic rocks is much larger, rising to 331 from which 275 are distributed in two large massifs (Făgăraș and Iezer), and the remaining are spread in 6 units characterized by gentler topography and lower altitude (Fig. 3a, Table 2). The northern direction clearly dominates in

both clusters, summing 41% from the total RW number, with similar frequencies on the NW and NE bins (Fig. 3d). The second highest RW frequency corresponds to the eastern orientation (104 RW), followed by the western slopes (77 RW). RW mapped on the southern slopes are scarce and represent 5.4% from the total number. In the large metamorphic massifs of Făgăraș and Iezer the highest RW density is in the range of 2100 – 2400 m with a mean altitude of 2200 m (Table 2), but 14 mapped surfaces are higher than 2400 m.

	Units	Main Rock Types	RW count	Mean Area (m^2x10^3)	Total Area (m^2 $x10^3$)	Mean Height (m)	Mean Slope (degrees)	Mean Alt (m)
Eastern C.	Călimani	Volcanic	5	4.79	23.97	35.8	39	1984
	Ceahlău / Hășmaș / Ciucaș	Limestone	6	59.45	356.71	162.5	44	1546
		Conglomerate	47	41.82	1965.95	83.5	35	1645
	Maramureș / Rodna	Schist	24	15.81	379.55	55.4	44	1950
		Volcanic	6	7.60	45.63	69.7	38	1799
	Bucegi	Conglomerate	42	116.16	4878.94	221.1	46	2096
		Limestone	7	72,5	507.51	175.5	48	1935
	Piatra Craiului	Limestone	13	220.82	2870.74	266.5	44	1967
	Făgăraș / Iezer	Schist	275	8.0	2200.78	73.1	41	2200
	Parâng / Retezat	Granite	175	12.5	2162.87	68.0	38	2229
		Schist	52	22,94	1193.22	95.7	40	2169
Southern C.	Buila / Piule-Iorgovanul / Țarcu / Cerna Valley	Limestone	70	34.1	1909.46	124.2	46	1346
		Conglomerate	17	14.38	244.47	59.3	41	1748
		Schist	8	8.75	70.04	65.3	46	1666
		Volcanic	2	4.83	9.67	46.0	39	1967
	Cozia / Cindrel / Șureanu / Lotrului / Căpățânii / Godeanu	Schist	56	4.61	258.25	33.0	38	1916

Table 2: The averaged values of the morphometric parameters and total cumulated area of the mapped RW in EC and SC

Parâng and Retezat Mts. in the SC (Fig. 1 for location) are two examples of mixed lithology, being composed mainly of granitoids plus granodiorites intrusions and of crystalline schist, micaschist, amphibolite (around 23% of the mapped surfaces) (Tables 1, 2) (Fig. 3b). Approximately 54% of the RW from Parâng and Retezat Mts. are North–oriented. Eastern and western exposures account for 25% and 15% of the total number, and only 5.7% of the mapped surfaces from the two massifs were identified on the southern slopes. More than half of the RW are concentrated in the 2100 – 2300 m interval and almost 18% extend above 2300 m, the northern ones reaching the highest altitudes. The RW on metamorphic rocks in the two massifs

range at slightly lower altitudes and occur almost evenly on the East, North and West–oriented slopes.

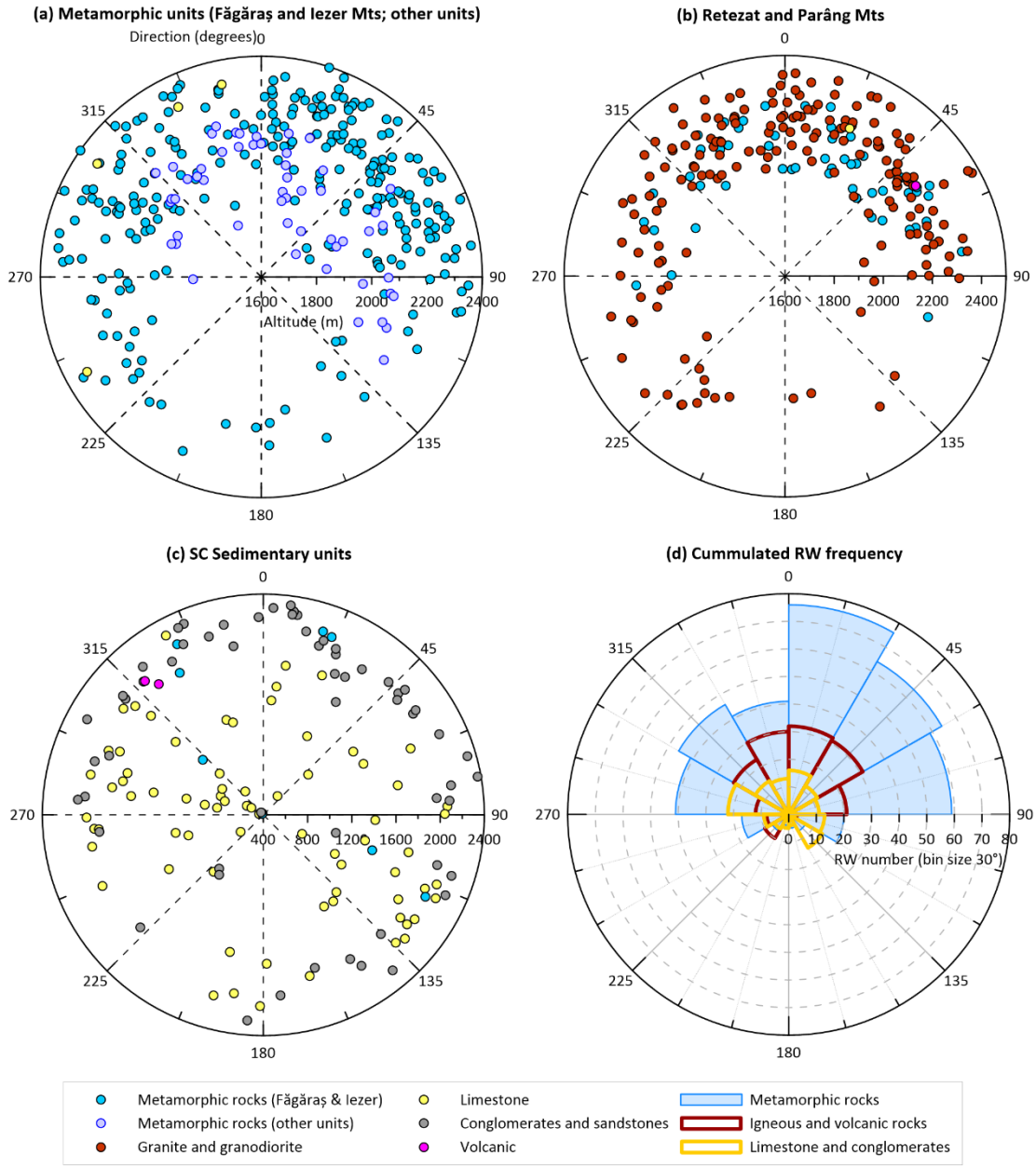

Figure 3: Direction and mean altitude of the RW mapped in the SC: (a) Făgăraș and Iezer Mts., with the secondary cluster of RW mapped in the lower altitude SC metamorphic units; (b) distribution of igneous and metamorphic rock surfaces in Parâng and Retezat Mts.; (d) distribution of limestone, conglomerate and sandstone RW mapped in SC; (d) Cumulated RW distribution on the four main rock categories represented on 30 degrees direction bins (please refer to the colour version)

In the limestone–prevailing units from the SC, (Bădescu and Tîrlă, 2020; see Fig. 1 for location), 69 RW were mapped (Fig. 3c), of which almost 40% are exposed towards West directions, 26% to the East, 23% are on northern slopes, and 11% on the southern ones (Fig. 3d). In terms of altitudinal distribution, there are also major discrepancies between the massifs, imposed by the structural characteristics of each (Table 1). The highest mean altitude is recorded in Piatra Craiului (1970 m) while Cerna Valley reaches the lowest (771 m).

Bucegi is the highest sedimentary massif (2507 m) from Carpathians, with most RW developed on conglomerates and sandstones, and 15% on limestone outcrops. RW are distributed mainly on the northern slopes (37%) and only 16% are South–facing. Maximum RW density is between 2100 and 2300 m for the North and East–exposed slopes. East, South and West RW are situated at lower elevations and occur on a wider altitudinal range (1800 – 2200 m).

The statistical analysis shows the clear dominance of West–exposed RWs for most of the considered morphometric parameters compared to the other main orientations (Table 3). This asymmetry is however case–specific and imposed by the particular orientation of many of the sedimentary units, respectively the NNE–SSW–oriented ridges and plateaus of Piatra Craiului and Buila hogbacks, Bucegi, Ciucaș and Hășmaș synclines (Mutihac, 1990) or Cerna Valley half–graben (Povară *et al.*, 2013), which together with the eastward and southward dipping strata contribute to the larger occurrence of West and North–exposed RWs (Fig. 1b).

Ratio	Mean area	Height	Altitude
N/E	2.38 (**)	2.36 (**)	3.19 (***)
S/E	1.11 (·)	1.33 (·)	-3.7 (***)
W/E	5.34 (***)	5.71 (***)	-2 (*)
S/N	-0.41 (·)	-0.17 (·)	-6.05 (***)
W/N	3.66 (***)	4.1 (***)	-5.27 (***)
W/S	2.76 (**)	2.83 (**)	2.18 (*)

Table 3: Results of the statistical analysis (Post–Hoc Dunn's Test) of morphometric parameters for pairs of main exposures. Numbers represent the z-Score, which indicates whether the tested parameter pair has a value above the rank mean (positive value), or below (negative value). For example, the mean area of N/E pair has a z-Score = 2.38, meaning that North has a greater mean area than East. In a similar way, for z-Scores below the rank mean the

comparison is read inversely, as in the altitude for S/N pair which has a z-Score = -6.05, meaning that North has a higher altitude than South

* p–value (0.05, 0.01]; ** p–value (0.01, 0.001]; *** p–value < 0.001. A p–value < 0.05 indicates a strong statistical significance at 95% confidence level

Ratio	Area	Height	Altitude
Conglomerate/ Limestone	-1.78 (*)	-3.9 (***)	2.93 (**)
Granite/ Limestone	-7.54 (***)	-6.9 (***)	12.89 (***)
Schist/ Limestone	-9.01 (***)	-8.36 (***)	10.9 (***)
Granite/ Conglomerate	-5.99 (***)	-2.79 (**)	10.31 (***)
Schist/ Conglomerate	-7.46 (***)	-3.87 (***)	7.91 (***)
Schist/ Granite	-0.77 (·)	-0.83 (·)	-4.53 (***)

Table 4: Results of the statistical analysis (Post–Hoc Dunn's Test) of morphometric parameters for pairs of main exposures. Numbers represent the z-Score, which indicates whether the tested parameter pair has a value above the rank mean (positive value), or below (negative value)

* p–value (0.05, 0.01]; ** p–value (0.01, 0.001]; *** p–value < 0.001. A p–value < 0.05 indicates a strong statistical significance at 95% confidence level

In summary, our observations indicate that RW in metamorphic and igneous units are generally restricted to altitudes higher than 2100 m, show a high density on the North–exposed slopes and lack from the southern ones. In comparison, RW distribution in sedimentary units is spread over a larger range of altitudes but highly dependent on the structure and strata dip-direction which result in prevalent West and North exposures but not as large (asymmetric) as for the metamorphic and igneous rocks.

4.2 RW morphometry

Although the most numerous RW were identified on metamorphic rocks, this group covers only 21% of the total mapped surface. An even smaller cumulated area corresponds to igneous rocks which represent 12% of the total area. Comparatively, although counting less RW, the sedimentary massifs cumulate 67% of the total mapped area due to their large mean surface (Fig. 4a, b). Consequently, igneous and metamorphic RW are 5 to 6 times smaller than limestone, conglomerates and sandstone RW (Fig. 5a).

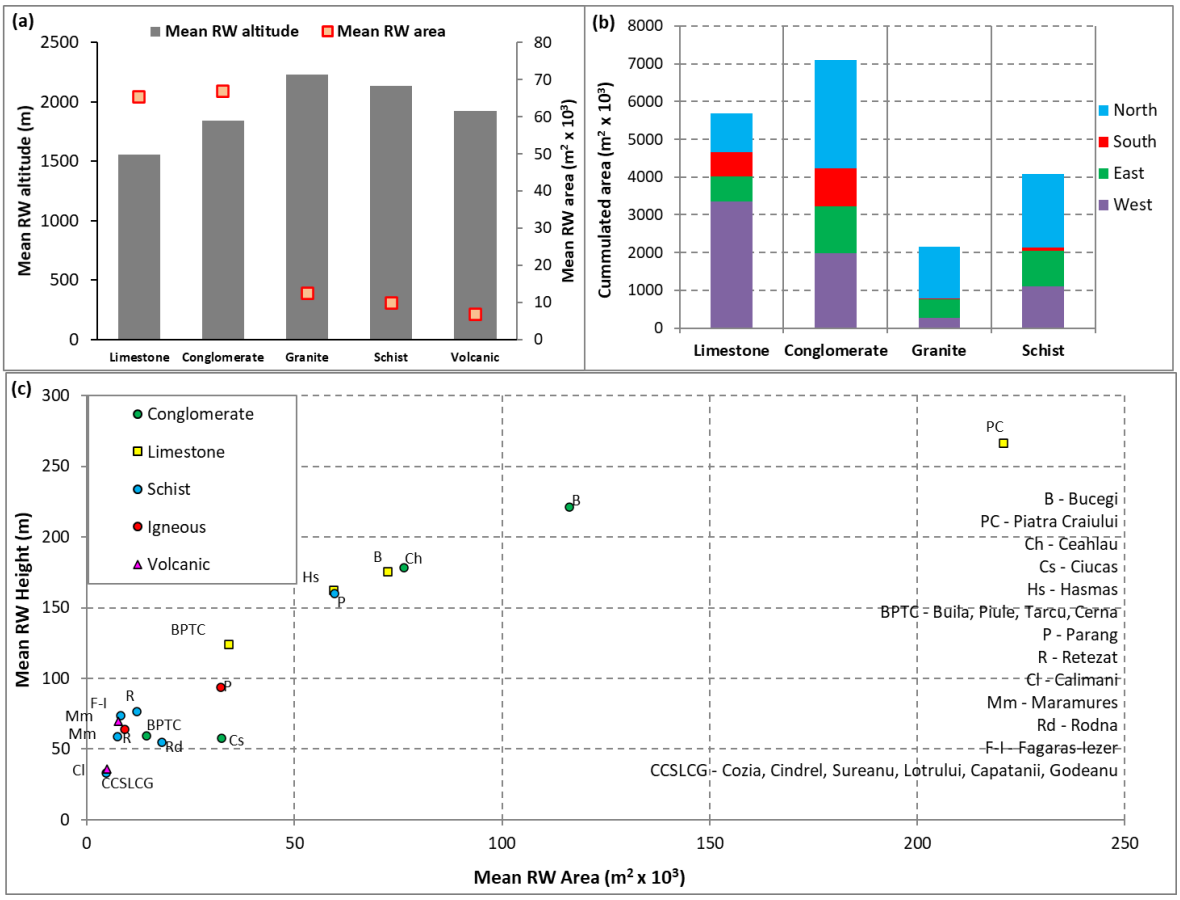

Figure 4: General RW morphometry on the main rock types (counting all features corresponding to the same rock type): (a) Mean RW altitude vs mean RW area; (b) Cumulated area of RW with the same lithology grouped on the four main cardinal directions; (c) Mean RW height and area derived for each massif (please refer to the colour version)

Metamorphic and igneous units are relatively similar in terms of RW vertical extension (around 70 m in average) and show little inter–site variation whereas the sedimentary units both for limestone, conglomerate and sandstone RW reach almost double height values (Fig. 4c, 5b). This visible heterogeneity is imposed by Bucegi and Piatra Craiului, with RW of up to 250 m height. This is also consistent with the wider range of mean RW altitude, as limestone surfaces extend at much lower altitudes (Fig. 5c).

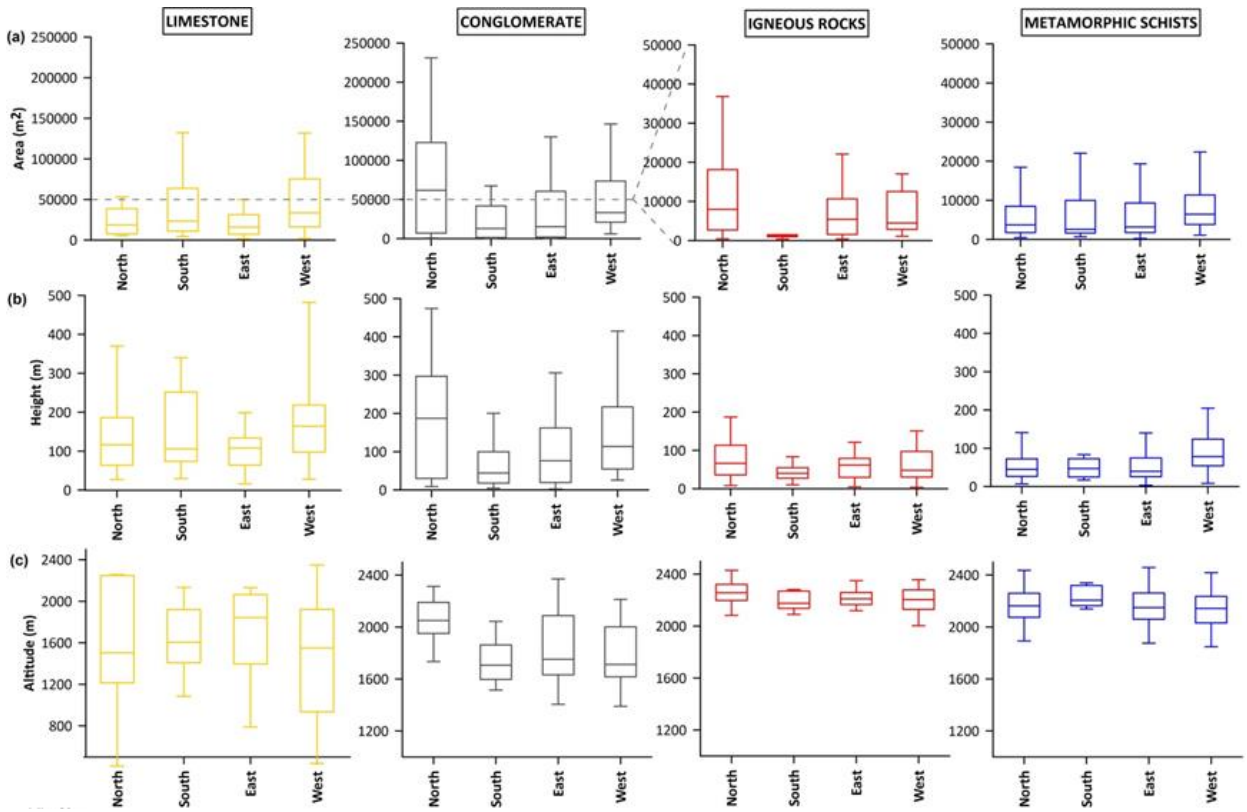

Figure 5: Variability of the morphometry of the RW grouped in the main lithological classes in respect to the main orientations: (a) mean RW area; (b) mean height; (c) mean altitude. The boxes display the median values, the 25–75 quartiles (lower – upper) and the caps show the minimum and maximum values (1.5 IQR)

Summing up, the high values of the z-scores in Table 4 (maximum -9.01 for schist/limestone area, 10.9 for mean altitude) support the high morphometric differences that exist between the sedimentary units and the metamorphic and igneous ones, which are more similar (-0.77 for schist/granite area, -4.3 for altitude). Although more numerous, metamorphic and igneous RW in the study area present typically small–size surfaces perched to the highest stands of formerly glaciated valleys and cirques. The sedimentary (limestone and conglomerates prevailing) RW are wider, steeper and cover larger areas than all the other lithological groups independent of glacial landmarks and with apparent homogeneity in respect to slope orientation. These characteristics thus reflect major differences between control factors over RW morphometry and distribution depending on geology.

4.3 Absolute ages

Sample locations, altitudes, ^{10}Be concentrations and ^{10}Be surface exposure ages determined in this study and selected from the literature are presented in Table 5. Multiple values (3 to 5 per valley) available in 8 of the valleys presented here, allowed an intra and inter-massif analysis of age distributions. Values range between 0.97 ± 0.08 ka and 11.3 ± 1.0 ka (Table 5), clustering between 11.3 and 9.1 ka (21 values), thus immediately following the Younger Dryas (12.9–11.7 ka, Rasmussen et al., 2006; 12.6–11.4 ka, Tămaş et al., 2005) and within time lags of up to 2.6 ka after. A second high frequency cluster was found between 9.0 and 7.0 ka, while younger ages were identified with a frequency of 1.75 values/1000 yrs. There is not a clear correlation between the absolute ages of the rock surfaces and the altitude. Such an attempt would be hindered by the unequal sample distribution, given the fact that most of the boulders are situated above 1800 m a.s.l. Nevertheless, most of the youngest ages (0.94 ± 0.08 ka, 4.51 ± 0.18 ka, 2.19 ± 0.12 ka, 1.27 ± 0.22 ka) were found in the lower or mid-sectors of Dejani, Bâlea and Sâmbăta valleys (Făgăraș Mts.), between 1200 and 1500 m a.s.l., respectively. Although few ages from the onset of the Holocene were also determined below 1400 m in the Retezat and Parâng Mts., (10.7 ± 1.4 ka, Ruszkiczay-Rüdiger *et al.*, 2021, 10.5 ± 0.9 ka, Gheorghiu *et al.*, 2015), most boulders dating between 11.5 and 7.0 ka are situated in the highest sector of the valleys and on cirque floors (1800–2200 m a.s.l.). This distribution pattern is similar when comparing both valleys within the same massif (e.g., Făgăraș) and valleys from the five different massifs (Table 5).

The samples from Doamnei rock glacier yielded values of 12.97 ± 0.38 and 11.44 ± 0.34 ka in the front sector, which gradually decrease to 9.91 ± 0.45 in the middle part and 3.37 ± 0.10 ka at RW base. The exposure date of the source RW and the youngest rock glacier boulder age from the upmost sector indicate rockfalls activity during Late Holocene (Table 5). Comparatively, the South-exposed side of the ridge has returned a much older age (52.64 ± 0.89 ka).

LOCATION	Sample name	Lat	Long	Altitude (m)	Quartz mass (g)	[^{10}Be] atoms g^{-1} x 10^4	t (exposure time) ka	Source
FĂGĂRAȘ								
Arpaș	AR01	45.60	24.67	2134	23.23	8.76 ± 0.33	4.07 ± 0.13	this study[a]
Bâlea Valley	BL	45.64	24.60	1205	24.39	4.92 ± 0.18	4.51 ± 0.18	
Dejani Valley	DEJ01	45.61	24.94	1300	23.05	1.13 ± 0.10	0.97 ± 0.08	
Dejani Valley	DEJ02	45.61	24.94	1287	26.72	8.15 ± 0.31	7.11 ± 0.26	
Dejani Valley	DEJ03	45.59	24.94	1929	26.00	16.91 ± 0.63	9.11 ± 0.34	
Dejani Valley	DEJ04	45.60	24.94	1401	25.77	13.36 ± 0.50	10.55 ± 0.39	
Fundul Caprei Valley	FC02A	45.60	24.64	1850	23.11	15.71 ± 0.59	9.04 ± 0.33	
Mioarele cirque	MIO01	45.58	24.83	2287	26.41	24.28 ± 0.91	10.14 ± 0.38	
Mioarele cirque	MIO02	45.58	24.83	2274	22.88	24.18 ± 0.76	10.14 ± 0.31	
Mioarele	MIO03	45.58	24.83	2285	24.74	24.33 ± 0.91	10.15 ± 0.38	
Orzăneaua cirque	ORZ02	45.60	24.72	1985	25.55	16.98 ± 0.64	8.79 ± 0.33	
Sâmbăta Valley	VS02	45.61	24.80	1823	25.11	16.60 ± 0.62	9.65 ± 0.36	
Sâmbăta Valley	VS01	45.61	24.80	1796	23.66	16.77 ± 0.57	9.95 ± 0.33	
Sâmbăta Valley	SA07	45.64	24.79	1215	26.22	2.46 ± 0.09	2.19 ± 0.12	
Sâmbăta Valley	SA05	45.62	24.79	1485	14.56	1.87 ± 0.07	1.27 ± 0.22	
Sâmbăta Valley	SA04	45.36	24.47	1820	-	-	10.00 ± 0.30	
Urlea cirque	U04	45.60	24.84	2077	25.44	16.00 ± 0.60	7.92 ± 0.29	
Urlea cirque	U01	45.60	24.84	2134	22.88	19.68 ± 0.59	9.36 ± 0.28	
Urlea cirque	U06	45.60	24.85	2062	27.87	22.14 ± 0.83	10.86 ± 0.40	
Urlea cirque	U01A	45.60	24.84	2130	23.07	22.94 ± 0.86	10.95 ± 0.41	
Doamnei RW N	DBEN	45.35	24.36	2230	20.48	3.59 ± 0.24	2.07 ± 0.13	
Doamnei RW S	DBES	45.35	24.36	2243	20.24	121.18 ± 2.06	52.46 ± 0.89	
Doamnei RG1	DBE1	45.36	24.36	2057	20.33	20.39 ± 0.94	9.91 ± 0.45	
Doamnei RG2	DBE2	45.36	24.36	2062	20.61	26.71 ± 0.79	12.97 ± 0.38	
Doamnei RG3	DBE3	45.36	24.36	2082	21.07	23.88 ± 0.71	11.44 ± 0.34	
Doamnei RG4	DBE4	45.35	24.36	2133	20.70	7.01 ± 0.22	3.37 ± 0.10	
BUCEGI								
Gaura Valley	Gaura05	45.43	25.40	1541	25.41	15.76 ± 0.61	10.78 ± 0.43	
Gaura Valley	Gaura06	45.43	25.40	1545	25.74	15.50 ± 0.46	10.62 ± 0.33	
Gaura cirque	Gaura03	45.44	25.43	2072	15.44	15.72 ± 0.49	7.49 ± 0.23	
Gaura cirque	Gaura01	45.44	25.43	2081	25.39	15.60 ± 0.53	8.00 ± 0.25	
PARANG								
Iezer Valley	PR01	45.34	23.63	2034	10.99	24.34 ± 1.08	11.20 ± 0.50	Gheorghiu *et al.* (2015)[b]
Iezer Valley	PR03	45.34	23.62	1970	14.33	13.61 ± 0.46	6.20 ± 0.20	
Iezer Valley	PR05	45.34	23.62	2008	10.6	19.64 ± 0.63	8.80 ± 0.80	
Gâlcescu cirque	PR10	45.35	23.61	1990	8.21	24.29 ± 0.69	11.20 ± 0.30	
Zănoaga Mare cirque	PR15	45.35	23.59	2055	10.19	23.63 ± 0.70	10.20 ± 0.30	
Zănoaga Mare cirque	PR16	45.35	23.59	2055	10.56	23.94 ± 0.83	10.40 ± 0.30	

Table 5: Sampling locations, ^{10}Be concentrations, and ^{10}Be surface exposure ages for post–Younger Dryas dated boulders in the Romanian Carpathians

[a] Analytical uncertainties (reported as 1-σ) included for all samples. No corrections for potential effects of snow cover or denudation were applied to the ages

[b] Exposure ages calculated using Cronus-Earth 10Be - 26Al exposure age calculator v. 2.2 (http://hess.ess.washington.edu/). They assume zero erosion, scaling factors according to Stone (2000) and a spallation production rate of 4.49 ± 0.39 atom (g SiO2) -1 a-1 (Balco *et al.*, 2008). Exposure ages are presented with the external uncertainties

RETEZAT								
Lăpușnicu Valley	Re15-29	45.31	22.78	1167	-	10.30 ± 0.13	10.70 ± 1.40	Ruszkiczay-Rüdiger *et al.*, (2021)[c]
Pietrele Valley	Pt-03-02	45.28	22.88	1902	-	23.9	11.40 ± 1.30	Reuther *et al.* (2007)[d]
RODNA								
Pietroasă Valley	RD 30	47.61	24.64	1379	25.11	16.32 ± 0.50	10.50 ± 0.90	Gheorghiu, (2012)[ee]
Zănoaga Mare cirque	RD 04	47.6	24.64	1669	28.95	21.65 ± 0.63	11.50 ± 1.00	
Zănoaga Mare cirque	RD 06	47.6	27.63	1767	24.24	22.83 ± 0.63	11.30 ± 1.00	
Zănoaga Mare cirque	RD 07	47.6	27.63	1767	25.85	22.50 ± 0.65	11.10 ± 1.00	
Zănoaga Mare cirque	RD 05	47.6	27.63	1753	24.36	10.89 ± 0.40	5.70 ± 0.50	
Buhăiescu Valley	RD 19	47.58	24.65	1718	23.01	21.61 ± 0.63	10.40 ± 0.90	

[c] The measured 10Be/9Be AMS ratios were corrected for full processed blank ratios: (3.30±0.50) x 10^{-15}. Age uncertainties: the 1st number is the internal uncertainty (AMS measurement, weighting, carrier, blank and half-life; 1-σ). Every reported age was corrected for topographic- and self-shielding

[d] Exposure age corrected for the effect of topographic shielding and surface geometry

[e] Exposure ages calculated using Cronus-Earth 10Be – 26Al exposure age calculator v. 2.2 (http://hess.ess.washington.edu/). They assume zero erosion, scaling factors according to Stone (2000)

5. DISCUSSION

5.1 Structure and lithology influence on RW distribution

The RW inventory and morphometric analysis results have emphasized the significant influence of the lithology and geological structure on the characteristics of metamorphic, igneous and sedimentary RW in the Romanian Carpathians, the first two rock categories producing much smaller RW, but developed at higher altitudes, than sedimentary massifs which account for the greatest rock surface coverage overall. Our results also showed that the distribution of RW in the Carpathians is very particular in respect to orientation, with an obvious asymmetry between North and South exposures especially for metamorphic and igneous rocks, yet with extent RW on all orientations in limestone or conglomerate massifs.

Despite the North / South balanced distribution of the glacial cirques (Mîndrescu, 2016), we showed that RW present a high asymmetry in the metamorphic and igneous mountain units from the both SC and EC (Fig. 2a, 4b, d), where South–exposed slopes are much less frequent whilst the total covered area is almost 30 times higher on the North–exposed RW.

Correspondently, the present rock glaciers distribution in these units accounts for 58% of the mapped rock glaciers in the northern quadrant, and only 13% in the southern one (Onaca *et al.*, 2017), which also suggests a more intense/frequent debris accumulation on the North exposed slopes during Younger Dryas and Early Holocene when presumably most of the rock glaciers formed (Onaca *et al.*, 2013). A similar distribution is described in the Adamello–Presanella massif (Italian Alps), where the main ridge follows the NE-SW direction of the North-bordering fault and valleys radiate from the main ridge, covering all the cardinal directions. Here, based on the inventory of 216 rock glaciers mostly consisting of intrusive granodioritic and tonalitic rocks, Baroni et al., (2004) show that both active and relict rock glaciers are predominantly facing the North, NW and NE compared to the southern quadrant (which counts 18% of the active / inactive, and 15% of the relict ones), and argument, by comparing front altitudes, that local topoclimate makes northern slopes more favourable to rock glacier formation and preservation. We further consider that RW preservation conditions are also more restrictive on the southern slopes in igneous and metamorphic slopes, as commented below.

Both granite and schist RW in the study area are characterized by metric joints networks which fit well with the dimensions of the boulders enclosed into the adjacent debris deposits (Vasile and Vespremeanu-Stroe, 2017), supporting intense slope modelling which could have led to the formation of large debris deposits, talus cones and rock glaciers. In a simulation of moisture availability in alpine RWs, (Rode et al. 2016) highlight that the preconditions of water saturation and temperature required for ice segregation are often recorded on the North-exposed slopes but just rarely met on warmer South–exposed rock surfaces, which implies that the latter are not prone for large–size debris production. Thus, South–exposed rock slopes would be subject to small–scale flake and granular rock shattering under the effect of both superficial freezing during snow melting intervals (Matsuoka, 2008) and of diurnal insolation thermal stress during snow–free intervals (Eppes *et al.*, 2016). We assume that South–exposed RW in the Romanian Carpathians were generally more stable than the other exposures whilst the northern were the

most active due to longer permafrost preservation. This is also supported by the old age (52.46 ± 0.89 ka) age yielded by the South-exposed ridge outcrop above Doamnei rock glacier, which was apparently unaffected by LGM, when it most probably stood as nunatak. Humification process (i.e. humus formation in soil profiles) has been inferred to be more intense on South–exposed mountain slopes, where warmer conditions intensify oxidation and create a more optimal environment for microorganisms that degrade organic matter (Egli *et al.*, 2010), compared to North–exposed mountain slopes which incorporate undecomposed or weakly degraded organic matter and are subject to mineral leaching due to colder and wetter conditions. Savi et al. (2015) reconstruct frost-cracking intensity and debris production during the Holocene in the Eastern Italian Alps, and emphasizes that high debris accumulation occurred during Early Holocene and also during Atlantic and Subatlantic periods when positive MAAT would have promoted continuous superficial (up to 100 cm deep) frost cracking in the highest peaks (around 3000 m a.s.l.). A similar pattern is supported in the SC by the surface exposure ages that sustain production of large debris in all massifs during Early Holocene and secondary debris production in subsequent phases.

The cumulated effect of these processes could explain a generally faster cover with soil and vegetation on the sunny slopes of both metamorphic and igneous units from this study, whereas on the North, colder thermal regime and the production of large–size boulders led simultaneously to a better preservation of RW, which is reflected in present–day distribution and morphometry.

The large synclines represented by Bucegi and Ciucaș Mts., with main North to South dip direction of the conglomerate and sandstones bedding planes uplifted large RW on the North–facing cuesta fronts, typical for sedimentary units formed as synclines, perched synclines, or hogbacks which are generally dominated by the compactness and steepness of the cuesta escarpments (Huggett, 2007). This is also the case in the NE–SW–dipping limestone massifs in SC which enhanced the development of the largest RW on their western slopes. Limestone RW

in both EC and SC generally lack dense superficial joint networks which, along with increased permeability, limits water availability within the first centimetres of rock and implicitly turns ice segregation less probable, which implies reduced RW modelling by frost shattering and debris accumulation in sedimentary massifs (Johnson et al., 2007). This is reflected by the low number of rock glaciers formed / identified in the SC on sedimentary rocks (only 15 on limestone from a total statistical population of 306 rock glaciers; Onaca et al. 2017). Therefore, we consider the lithology and structure to play the major role in imposing the orientation–related homogeneity which accounts as the primary control in RW distribution and dimensions in the sedimentary units from this study. Secondary, post-glacial RW relaxation would have led to the detachment of massive limestone and conglomerate blocks as sustained by the absolute ages obtained in Bucegi Mts (Table 5). However, in specific cases, such as Piatra Craiului limestone hogback, large debris deposits have accumulated at the base of the main tectonic slopes. For such cases, we assume that the absence of transversal valleys and of the Pleistocene glaciers, both caused by topography, could have created the conditions for the long–term (e.g. Middle to Late Quaternary) debris accumulation, the formation of which is still to be deciphered.

5.2 Holocene dynamics of RW depicted by rock-slope failures

Following Last Glacial Maximum deglaciation (19-14.5 ka), small glaciers re-occupied the highest cirques (> 2050 m) during Younger Dryas excepting the southern ones (Gheorghiu *et al.*, 2015; Popescu et al., 2017a; Pascal et al., 2018). The largest Younger Dryas glaciers are likely to have lasted more than a millennium during Early Holocene (e.g. 10.2 ± 0.9 kyrs, Gheorghiu *et al.*, 2015). Therefore, we consider that most of the boulders from high altitudes (> 2000 m) of early Holocene age dated in this study have originated by RW destabilization as response of ice retreat which occurred mainly in the upper valley/cirques sectors where glaciers were restricted (Fig. 6). High frequency of such events occurring several thousand years after Younger Dryas period are well documented in the European Alps (Soldati et al., 2004; Cossart *et al.*, 2008; Hormes *et al.*, 2008; Prager *et al.*, 2008; Ivy-Ochs *et al.*, 2009), Tatra Mts. (Pánek

et al., 2016), in Scotland (Ballantyne *et al.*, 2014) and Scandinavia (Mercier *et al.*, 2013; Hilger *et al.*, 2018, 2021; Vick *et al.*, 2022), but also in Karakorum (Shroder *et al.*, 2011) or the Andes (Fauqué et al., 2009). Many of these sites record re-activations or secondary clusters during the Sub-Boreal period (Hermanns and Longva, 2013).

In Fig. 6 we compare frequency curves of the post Younger Dryas boulders dated in the Romanian Carpathians and of the RSF ages compiled from these studies after excluding the mountain ranges which are influenced by excess of humidity/dryness and correspondently by their variability in time (e.g., Himalaya, Atlas or Cascade Mts). Overall, the Romanian Carpathians show a similar general trend with the other world-wide catenae but with an apparently more rapid and accentuated response to the Early Holocene warming and more humid conditions, so that almost 3/4 of the dated RSF occurred before 8 ka with the highest frequency window positioned during 11.6-9 ka. Conversely, the multi-sites curve reflects a higher sensitivity of RW (deduced via RSF occurrence) to the Holocene Climatic Optimum, which can be explained both by delays in local deglaciation momentum and topoclimatic conditions. Given the relatively small number of samples used in our study (38), this first attempt to assess the RSF evolution in the Romanian Carpathians might also be biased towards the Early Holocene by the high frequency of the high-altitude samples (71% of the samples are >1700 m). As future research, it is necessary to expand the RSF dating by including more cases from the mid and low levels and to compare their histories in order to disentangle the influence of deglaciation, permafrost thawing, thermal and humidity variation. However, some of the European studies describe some similar results with the newly-obtained in the Romanian Carpathians, such as Hermanns and Longva (2013) which give an estimation of Holocene RSF magnitude in Storfjörden, Norway, showing that the earliest events (12.5 to 10 kyrs) generated by far the largest detached volumes (Fig. 6), compared to the ones dating after 8 kyrs. Similarly, reconstructed magnitudes of large landslides from the Alps (Soldati et al., 2004; Ivy-Ochs *et al.*, 2009), place such events in the first millennia of the Holocene.

Independently of the absolute exposure ages used to assess the RSF probability occurrence during Holocene (Fig. 6), the other four surface ages from Doamnei rock glacier, in the central Făgăraș massif, indicate multiple phases of debris accumulation, and, in the same time, the high magnitude of early–Holocene debris production, which supplied at least the lower half of the rock glacier body, demonstrated by the rapid accumulation of massive boulders as well as their displacement between 12.97 and 9.91 ka ago. RW permafrost decay would have further enhanced subsequent rockfall or rock avalanches of smaller magnitude during the following warm episodes of the Holocene as also described in the Swiss Alps by Nagelisen *et al.*, (2015). The particularly large boulders in the lower half of Doamnei rock glacier are incompatible with frost-cracking intensities estimated for the Holocene (Savi et al., 2015) and were most probably produced by similar high magnitude (as described by Hermanns and Longva, 2013) slope failures induced by slope relaxation, permafrost degradation and overall weakened slope coherence. We consider this to be the ultimate process/interval of intense modelling in the alpine area of the Carpathians which defined the rock walls – rock glaciers/debris systems preserved until present.

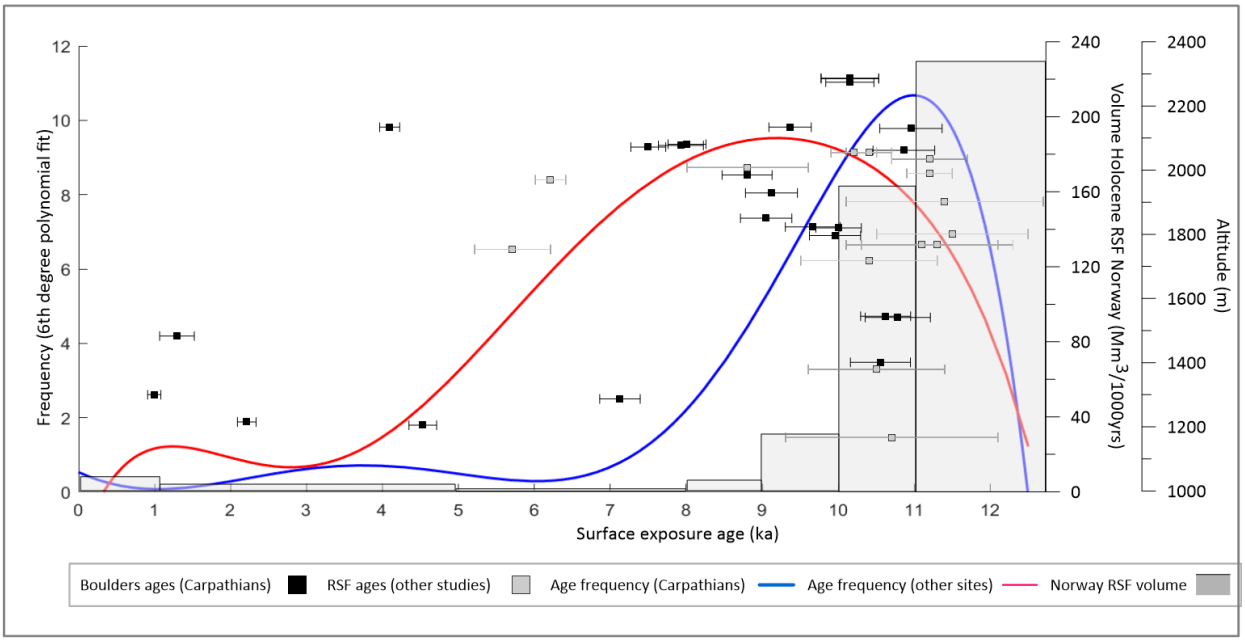

Figure 6 Cumulated distribution of surface exposure ages attributed to post-Younger Dryas RSF in the Romanian Carpathians (blue line), and multi-site composed RSF distribution (red line) using absolute ages from the French Alps (Cossart *et al.*, 2008), Swiss Alps (Ivy-Ochs *et al.*, 2009), Italian Alps (Hormes *et al.*, 2008), Central Andes (Fauque et al., 2009), Northern Iceland (Mercier *et al.*, 2013), Central Karakoram (Shroder *et al.*, 2011), Scotland and NW Ireland (Ballantyne *et al.*, 2014). Grey-filled columns represent estimated volume of Holocene RSF in Norway (after Hermanns and Longva, 2013)

6. CONCLUSIONS

The distribution of RW mapped in the Southern and Eastern Carpathians depends mainly on the lithology, structure but also weathering processes. In the metamorphic and igneous units, it ultimately relates to geomorphological context, being mostly associated with glacial cirques and valleys headwalls. Most RW are therefore restricted to the highest ridge sectors, while their low heights and areas are explained as a consequence of the lithological predisposition to debris production, especially in permafrost degrading conditions during warming phases of the Early Holocene. The North/South asymmetry in rock glaciers distribution (also signalled in other mid-latitude ranges) is reflected by the lack of South-exposed RW. We assume more stable conditions prone to fine debris and soil formation on the southern slopes due to insolation and warmer conditions.

For the sedimentary RW, tectonics and the geological structure are the main controls to explain the occurrence of the large (wide and high) limestone and conglomerate RW in the Romanian Carpathians. Except for Bucegi Mts, which were high and large enough to host complex glaciers during the last glaciation, most of the sedimentary units from SC and EC were not subject to glacial erosion during LGM due to either steep topography (e.g., hogback ridges) or lower altitude, although RW permafrost was probably widespread.

Absolute exposure ages confirm that an intense rock slope degradation via rock-slope failures took place in the Carpathian metamorphic and igneous units in Early Holocene, similar with other European sites, reaching the highest magnitudes 11.6 – 9 ka ago especially above 1800

m altitude. We associate the present distribution of RW with this periglacially-active period which was the last time of rock surfaces substantial reshape.

Acknowledgements: The research financing these results received funding from the Norway Grants 2014-2021 (project code RO-NO-2019-0415 / contract no. 30/2020), from University of Bucharest grants (project code C1.2.PFE-CDI.2021-587) and from the Research Institute of the University of Bucharest fellowship for young researchers (2018-2019 grants, awarded to MV).

References

Allen, S. and Huggel, C. (2013) 'Extremely warm temperatures as a potential cause of recent high mountain rockfall', *Global and Planetary Change*, 107, pp. 59–69. doi: 10.1016/j.gloplacha.2013.04.007.

Ardelean, A. C. *et al.* (2017) 'Quantifying postglacial sediment storage and denudation rates in a small alpine catchment of the Făgăraș Mountains (Romania)', *Science of the Total Environment*, 599–600 (March 2018), pp. 1756–1767. doi: 10.1016/j.scitotenv.2017.05.131.

Ardelean, F. (2013) *Clasificarea semi-automată a unor forme de relief pentru cartarea geomorfologică. Studiu de caz Munții Țarcu*. West University of Timișoara.

Ardelean, F., Török-Oance, M. and Drăguț, L. (2012) 'Object-based detection of planation surfaces from Digital Elevation Models. Case study Țarcu Mountains, Southern Carpathians, Romania', in *Forum Carpathicum, From data to knowledge, from knowledge to action.*, pp. 127–128.

Bădescu, B. and Tîrlă, L. (2020) *Harta carstului din România, 2020*. Exploratorii, Asociația speologică.

Balco, G. *et al.* (2008) 'A complete and easily accessible means of calculating surface exposure ages or erosion rates from 10 Be and 26 Al measurements', 3, pp. 174–195. doi: 10.1016/j.quageo.2007.12.001.

Ballantyne, C. K. *et al.* (2014) 'Enhanced rock-slope failure following ice-sheet deglaciation: Timing and causes', *Earth Surface Processes and Landforms*, 39(7), pp. 900–913. doi: 10.1002/esp.3495.

Baroni, C., Carton, A. and Seppi, R. (2004) 'Distribution and behaviour of rock glaciers in the Adamello-Presanella massif (Italian Alps)', *Permafrost and Periglacial Processes*, 15(3), pp. 243–259. doi: 10.1002/ppp.497.

Bartosch, T., Stüwe, K. and Robl, J. (2017) 'Topographic evolution of the Eastern Alps: The influence of strike-slip faulting activity', *Lithosphere*, 9(3), pp. 384–398. doi: 10.1130/L594.1.

Borchers, B. *et al.* (2016) 'Geological calibration of spallation production rates in the CRONUS-Earth project', *Quaternary Geochronology*, 31, pp. 188–198. doi: 10.1016/j.quageo.2015.01.009.

Braucher, R. *et al.* (2003) 'In situ produced 10Be measurements at great depths: implications for production rates by fast muons', *Earth and Planetary Science Letters*, 211(3–4), pp. 251–258. doi: 10.1016/S0012-821X(03)00205-X.

Braucher, R. *et al.* (2011) 'Production of cosmogenic radionuclides at great depth: A multi element approach'. doi: 10.1016/j.epsl.2011.06.036.

Braucher, R. *et al.* (2015) 'Preparation of ASTER in-house 10Be/9Be standard solutions', *Nuclear Instruments and Methods in Physics Research Section B: Beam Interactions with Materials and Atoms*, 361, pp. 335–340. doi: 10.1016/J.NIMB.2015.06.012.

Chmeleff, J. *et al.* (2010) 'Determination of the 10Be half-life by multicollector ICP-MS and liquid scintillation counting', *Nuclear Instruments and Methods in Physics Research, Section B: Beam Interactions with Materials and Atoms*, 268(2), pp. 192–199. doi: 10.1016/j.nimb.2009.09.012.

Corona, C., Trappmann, D. and Stoffel, M. (2013) 'Parameterization of rockfall source areas and magnitudes with ecological recorders: When disturbances in trees serve the calibration and validation of simulation runs', *Geomorphology*, 202, pp. 33–42. doi: 10.1016/j.geomorph.2013.02.001.

Cossart, E. *et al.* (2008) 'Slope instability in relation to glacial debuttressing in alpine areas (Upper Durance catchment, southeastern France): Evidence from field data and 10Be cosmic ray exposure ages', *Geomorphology*, 95(1–2), pp. 3–26. doi: 10.1016/j.geomorph.2006.12.022.

Curry, A. M. and Morris, C. J. (2004) 'Lateglacial and Holocene talus slope development and rockwall retreat on Mynydd Du, UK', *Geomorphology*, 58(1–4), pp. 85–106. doi: 10.1016/S0169-555X(03)00226-5.

Dunn, O. J. (1961) 'Multiple Comparisons among Means', *Journal of the American Statistical Association*, 56(293), pp. 52–64. doi: 10.1080/01621459.1961.10482090.

Egli, M. *et al.* (2010) 'The effects of exposure and climate on the weathering of late Pleistocene and Holocene Alpine soils', *Geomorphology*, 114(3), pp. 466–482. doi: 10.1016/j.geomorph.2009.08.008.

Ellis, M. A. and Barnes, J. B. (2015) 'A global perspective on the topographic response to fault growth', *Geosphere*, 11(4), pp. 1008–1023. doi: 10.1130/GES01156.1.

Eppes, M. C. *et al.* (2016) 'Deciphering the role of solar-induced thermal stresses in rock weathering', *Bulletin of the Geological Society of America*, 128(9–10), pp. 1315–1338. doi: 10.1130/B31422.1.

Gheorghiu, D. M. (2012) 'Testing climate synchronicity between Scotland and Romania since the last glacial maximum', pp. 1–214. Available at: http://theses.gla.ac.uk/3362/.

Gheorghiu, D. M. *et al.* (2015) 'Deglaciation constraints in the Parâng Mountains, Southern Romania, using surface exposure dating', *Quaternary International*, 388(March 2016), pp. 156–167. doi: 10.1016/j.quaint.2015.04.059.

Girard, L. *et al.* (2013) 'Environmental controls of frost cracking revealed through in situ acoustic emission measurements in steep bedrock', *Geophysical Research Letters*, 40(9), pp. 1748–1753. doi: 10.1002/grl.50384.

Gruber, S. (2007) 'A mass-conserving fast algorithm to parameterize gravitational transport and deposition using digital elevation models', 43, pp. 1–8. doi: 10.1029/2006WR004868.

Gruber, S., Hoelzle, M. and Haeberli, W. (2004) 'Permafrost thaw and destabilization of Alpine rock walls in the hot summer of 2003', *Geophysical Research Letters*, 31(13), pp. 1–4. doi: 10.1029/2004GL020051.

Hales, T. C. and Roering, J. J. (2007) 'Climatic controls on frost cracking and implications for the evolution of bedrock landscapes', *Journal of Geophysical Research: Earth Surface*, 112(2), pp. 1–14. doi: 10.1029/2006JF000616.

Hermanns, R. L. and Hewitt, K. (2009) 'Aconcagua y su relación con depósitos asignados', (June 2014).

Hermanns, R. L. and Longva, O. (2013) 'Rapid rock-slope failures', *Landslides*, (January), pp. 59–70. doi: 10.1017/cbo9780511740367.007.

Hilger, P. *et al.* (2018) 'Multiple rock-slope failures from Mannen in Romsdal Valley, western Norway, revealed from Quaternary geological mapping and 10Be exposure dating', *Holocene*, 28(12), pp. 1841–1854. doi: 10.1177/0959683618798165.

Hilger, P. *et al.* (2021) 'Permafrost as a first order control on long-term rock-slope deformation in (Sub-)Arctic Norway', *Quaternary Science Reviews*, 251, p. 106718. doi: 10.1016/j.quascirev.2020.106718.

Hoeven, A. G. A. Van Der *et al.* (2005) 'Observation of present-day tectonic motions in the Southeastern Carpathians: Results of the ISES / CRC-461 GPS measurements', 239, pp. 177–184. doi: 10.1016/j.epsl.2005.09.018.

Hormes, A. *et al.* (2008) '10Be exposure ages of a rock avalanche and a late glacial moraine in Alta Valtellina, Italian Alps', *Quaternary International*, 190(1), pp. 136–145. doi: 10.1016/j.quaint.2007.06.036.

Huggett, R. J. (2007) *Fundamentals of Geomorphology*. Routledge.

Hughes, P. D., Gibbard, P. L. and Woodward, J. C. (2007) 'Geological controls on Pleistocene glaciation and cirque form in Greece', *Geomorphology*, 88(3–4), pp. 242–253. doi: 10.1016/j.geomorph.2006.11.008.

Iancu, S. (1970) *Masivul Parâng. Studiu Geomorfologic*. University of Bucharest.

Ivy-Ochs, S. *et al.* (2009) 'Surface exposure dating of the Flims landslide, Graubünden, Switzerland', *Geomorphology*, 103(1), pp. 104–112. doi: 10.1016/j.geomorph.2007.10.024.

Johnson, B. G., Thackray, G. D. and Van Kirk, R. (2007) 'The effect of topography, latitude, and lithology on rock glacier distribution in the Lemhi Range, central Idaho, USA', *Geomorphology*, 91(1–2), pp. 38–50. doi: 10.1016/j.geomorph.2007.01.023.

Krautblatter, M., Funk, D. and Günzel, F. K. (2013) 'Why permafrost rocks become unstable: A rock-ice-mechanical model in time and space', *Earth Surface Processes and Landforms*, 38(8), pp. 876–887. doi: 10.1002/esp.3374.

Kromer, R. (2017) 'Identifying and Monitoring Rockfall Precursors Using Terrestrial Laser Scanning for Improved Rockfall Hazard Management', p. 313. Available at: https://qspace.library.queensu.ca/handle/1974/22765.

Kruskal, W. H. and Wallis, W. A. (1952) 'Use of Ranks in One-Criterion Variance Analysis', *Journal of the American Statistical Association*, 47(260), p. 583. doi: 10.2307/2280779.

Lifton, Z. M. *et al.* (2009) 'Influence of rock strength on the valley morphometry of Big Creek, central Idaho, USA', *Geomorphology*, 111(3–4), pp. 173–181. doi: 10.1016/j.geomorph.2009.04.014.

Linzer, H. G. *et al.* (1998) 'Kinematic evolution of the Romanian Carpathians', *Tectonophysics*, 297(1–4), pp. 133–156. doi: 10.1016/S0040-1951(98)00166-8.

Loye, A., Jaboyedoff, M. and Pedrazzini, A. (2009) 'Identification of potential rockfall source areas at a regional scale using a DEM-based geomorphometric analysis', *Natural Hazards and Earth System Science*, 9(5), pp. 1643–1653. doi: 10.5194/nhess-9-1643-2009.

Magnin, F. *et al.* (2015) 'Determination of warm, sensitive permafrost areas in near-vertical rockwalls and evaluation of distributed models by electrical resistivity tomography', *Journal of Geophysical Research: Earth Surface*, 120(5), pp. 745–762. doi: 10.1002/2014JF003351.

Matsuoka, N. (2008) 'Frost weathering and rockwall erosion in the southeastern Swiss Alps: Long-term (1994-2006) observations', *Geomorphology*, 99(1–4), pp. 353–368. doi: 10.1016/j.geomorph.2007.11.013.

Matthews, J. A. *et al.* (2018) 'Small rock-slope failures conditioned by Holocene permafrost degradation: a new approach and conceptual model based on Schmidt-hammer exposure-age dating, Jotunheimen, southern Norway', *Boreas*, 47(4), pp. 1144–1169. doi: 10.1111/bor.12336.

McKight, P. E. and Najab, J. (2010) 'Kruskal-Wallis Test', *The Corsini Encyclopedia of Psychology*, pp. 1–1. doi: 10.1002/9780470479216.CORPSY0491.

Merchel, S. *et al.* (2008) 'Towards more precise 10 Be and 36 Cl data from measurements at the 10 À14 level: Influence of sample preparation', *Nuclear Inst. and Methods in Physics Research, B*, 266, pp. 4921–4926. doi: 10.1016/j.nimb.2008.07.031.

Merchel, S. and Herpers, U. (1999) 'An update on radiochemical separation techniques for the determination of long-lived radionuclides via accelerator mass spectrometry', *Radiochimica Acta*, 84, pp. 215–219.

Mercier, D. *et al.* (2013) 'The Höfǵ ahólar rock avalanche (sturzström): Chronological constraint of paraglacial landsliding on an Icelandic hillslope', *Holocene*, 23(3), pp. 432–446. doi: 10.1177/0959683612463104.

Merten, S. (2011) *Thermo-tectonic evolution of a convergent orogen with low topographic build-up: Exhumation and kinematic patterns in the Romanian Carpathians derived from thermochronology*. Vrije Universiteit Amsterdam. Available at: https://research.vu.nl/en/publications/thermo-tectonic-evolution-of-a-convergent-orogen-with-low-topogra.

Messenzehl, K. *et al.* (2017) 'Regional-scale controls on the spatial activity of rockfalls (Turtmann Valley, Swiss Alps) — A multivariate modeling approach', *Geomorphology*, 287, pp. 29–45. doi: 10.1016/j.geomorph.2016.01.008.

Micu, D. M. *et al.* (2015) *Climate of the Romanian Carpathians*. doi: 10.1007/978-3-319-02886-6.

Mîndrescu, M. (2016) *Geomorfometria circurilor glaciare din Carpații românești*. Editura Universității din Suceava.

Mîndrescu, M., Cristea, I. A. and Hutchinson, S. M. (2010) 'Bathymetric and sedimentological changes of glacial lake Ştiol, Rodna Masiff', *Carpathian Journal of Earth and Environmental Sciences*, 5(1), pp. 57–65.

Mîndrescu, M. and Evans, I. S. (2014) 'Cirque form and development in Romania: Allometry and the buzzsaw hypothesis', *Geomorphology*, 208, pp. 117–136. doi: 10.1016/j.geomorph.2013.11.019.

Mîndrescu, M., Evans, I. S. and Cox, N. J. (2010) 'Climatic implications of cirque distribution in the Romanian Carpathians: Palaeowind directions during glacial periods', *Journal of Quaternary Science*, 25(6), pp. 875–888. doi: 10.1002/jqs.1363.

Mutihac, V. (1990) *Structura geologică a teritoriului României*. Editura Tehnică.

Mutihac, V. (2004) *Gologia României*. București: Editura Didactică și Pedagogică.

Nagelisen, J. *et al.* (2015) 'Post-glacial rock avalanches in the Obersee Valley, Glarner Alps, Switzerland', *Geomorphology*, 238, pp. 94–111. doi: 10.1016/j.geomorph.2015.02.031.

Onaca, A. *et al.* (2013) 'Assessement of internal structure of periglacial landforms from southern carpathians (Romania) using dc resistivity tomography', *Carpathian Journal of Earth and Environmental Sciences*, 8(2), pp. 113–122.

Onaca, A. *et al.* (2015) 'Near surface thermal characteristics of alpine steep rockwalls in the Retezat Mountains', *Forum geografic*, XIV(2), pp. 124–133. doi: 10.5775/fg.2067-4635.2015.091.d.

Onaca, A., Urdea, P., *et al.* (2017) 'Present-Day Periglacial Processes in the Alpine Zone', in Rădoane, M. and Vespremeanu-Stroe,

A. (eds) *Landforms dynamics and evolution in Romania*. Springer International Publishing, pp. 147–176. doi: 10.1007/978-3-319-32589-7_7.

Onaca, A., Ardelean, F., *et al.* (2017) 'Southern Carpathian rock glaciers: Inventory, distribution and environmental controlling factors', *Geomorphology*, 293, pp. 391–404. doi: 10.1016/j.geomorph.2016.03.032.

Pánek, T. *et al.* (2016) 'Cosmogenic age constraints on post-LGM catastrophic rock slope failures in the Tatra Mountains (Western Carpathians)', *Catena*, 138(March), pp. 52–67. doi: 10.1016/j.catena.2015.11.005.

Phillips, M. *et al.* (2017) 'Rock slope failure in a recently deglaciated permafrost rock wall at Piz Kesch (Eastern Swiss Alps), February 2014', *Earth Surface Processes and Landforms*, 42(3), pp. 426–438. doi: 10.1002/esp.3992.

Popescu, R. *et al.* (2017) 'Spatial Distribution and Main Characteristics of Alpine Permafrost from Southern Carpathians, Romania', in Rădoane, M. and Vespremeanu-Stroe, A. (eds) *Landforms dynamics and evolution in Romania*. Springer International Publishing, pp. 117–146. doi: 10.1007/978-3-319-32589-7_6.

Popescu, R., Urdea, P. and Vespremeanu-Stroe, A. (2017) 'Deglaciation History of High Massifs from the Romanian Carpathians: Towards an Integrated View', in *Landforms dynamics and evolution in Romania*. Springer International Publishing, pp. 87–117. doi: 10.1007/978-3-319-32589-7_5.

Povară, I. *et al.* (2013) 'Water flow system within the Cerna Valley graben structure (SW of the Southern Carpathians, Romania)', in *International Symposium on Hierarchical Flow Systems in Karst Regions*.

Prager, C. *et al.* (2008) 'Age distribution of fossil landslides in the Tyrol (Austria) and its surrounding areas', *Natural Hazards and Earth System Science*, 8(2), pp. 377–407. doi: 10.5194/nhess-8-377-2008.

Reuther, A. U. *et al.* (2007) 'Late Pleistocene glacial chronology of the Pietrele Valley, Retezat Mountains, Southern Carpathians constrained by 10Be exposure ages and pedological investigations', *Quaternary International*, 164–165, pp. 151–169. doi: 10.1016/j.quaint.2006.10.011.

Rode, M., Schnepfleitner, H. and Sass, O. (2016) 'Simulation of moisture content in alpine rockwalls during freeze–thaw events', *Earth Surface Processes and Landforms*, 41(13), pp. 1937–1950. doi: 10.1002/esp.3961.

Ruszkiczay-Rüdiger, Z. *et al.* (2021) 'Limited glacial erosion during the last glaciation in mid-latitude cirques (Retezat Mts, Southern Carpathians, Romania)', *Geomorphology*, 384, p. 107719. doi: 10.1016/j.geomorph.2021.107719.

Săndulescu, M. (1984) *Geotectonica României*. Editura Tehnică.

Sauchyn, D. J., Cruden, D. M. and Hu, X. Q. (1998) 'Structural control of the morphometry of open rock basins, Kananaskis region, Canadian Rocky Mountains', *Geomorphology*, 22(3–4), pp. 313–324. doi: 10.1016/S0169-555X(97)00083-4.

Savi, S., Delunel, R. and Schlunegger, F. (2015) 'Efficiency of frost-cracking processes through space and time: An example from the eastern Italian Alps', *Geomorphology*, 232, pp. 248–260. doi: 10.1016/j.geomorph.2015.01.009.

Seong, Y. B. *et al.* (2009) 'Rates of basin-wide rockwall retreat in the K2 region of the Central Karakoram defined by terrestrial cosmogenic nuclide 10Be', *Geomorphology*, 107(3–4), pp. 254–262. doi: 10.1016/j.geomorph.2008.12.014.

Shapiro, S. S. and Wilk, M. B. (1965) 'An Analysis of Variance Test for Normality (Complete Samples)', *Biometrika*, 52(3/4), p. 591. doi: 10.2307/2333709.

Shroder, J. F. *et al.* (2011) 'The role of mass movements on landscape evolution in the Central Karakoram: Discussion and

speculation', *Quaternary International*, 236(1–2), pp. 34–47. doi: 10.1016/j.quaint.2010.05.024.

Soldati, M., Corsini, A. and Pasuto, A. (2004) 'Landslides and climate change in the Italian Dolomites since the Late glacial', *Catena*, 55(2), pp. 141–161. doi: 10.1016/S0341-8162(03)00113-9.

Stone, J. O. (2000) 'Air pressure and cosmogenic isotope production', *Journal of Geophysical Research: Solid Earth*, 105(B10), pp. 23753–23759. doi: 10.1029/2000JB900181.

Tămaş, T., Onac, B. P. and Bojar, A. V. (2005) 'Lateglacial-Middle Holocene stable isotope records in two coeval stalagmites from the Bihor Mountains, NW Romania', *Geological Quarterly*, 49(2), pp. 185–194.

Török-Oance, M. and Ardelean, F. (2012) 'Object-oriented image analysis for detection of the barren karst areas. A case study: the central sector of the Mehedinţi Mountains (Southern Carpathians)', *Carpathian Journal of Earth and Environmental Sciences*, 7, pp. 248–254.

Urdea, P. (2000) *Munții Retezat. Studiu Geomorfologic*. București: Editura Academiei Române.

Vaida, M. and Verniers, J. (2005) 'Biostratigraphy and palaeogeography of lower Devonian chitinozoans, from east and west Moesia, Romania', *Geologica Belgica*, 8(4), pp. 121–130.

Vasile, M. and Vespremeanu-Stroe, A. (2017) *Thermal weathering and distribution of mountain Rockwalls*, *Springer Geography*. doi: 10.1007/978-3-319-32589-7_8.

Vasile, Mirela and Vespremeanu-Stroe, A. (2017) 'Thermal Weathering and Distribution of Mountain Rockwalls', in Rădoane, M. and Vespremeanu-Stroe, A. (eds) *Landforms dynamics and evolution in Romania*. Springer International Publishing, pp. 177–196. doi: 10.1007/978-3-319-32589-7_8.

Vermeesch, P. (2007) 'CosmoCalc: An Excel add-in for cosmogenic nuclide calculations', *Geochemistry, Geophysics, Geosystems*, 8(8), p. 8003. doi: 10.1029/2006GC001530.

Vespremeanu-Stroe, A., Cheval, S. and Tătui, F. (2012) 'The wind regime of Romania – Characteristics, trends and North Atlantic oscillation influences', *Forum geografic*, XI(2), pp. 118–126. doi: 10.5775/fg.2067-4635.2012.003.d.

Vick, L. M. *et al.* (2022) 'Evolution and temporal constraints of a multiphase postglacial rock slope failure', *Geomorphology*, 398. doi: 10.1016/j.geomorph.2021.108069.

Willett, S. D. (1999) 'Orogeny and orography: The effects of erosion on the structure of mountain belts', *Journal of Geophysical Research: Solid Earth*, 104(B12), pp. 28957–28981. doi: 10.1029/1999jb900248.